



Universiteit  
Leiden  
The Netherlands

## Activity-based protein profiling of diacylglycerol lipases

Baggelaar, M.P.

### Citation

Baggelaar, M. P. (2017, April 6). *Activity-based protein profiling of diacylglycerol lipases*. Retrieved from <https://hdl.handle.net/1887/48284>

Version: Not Applicable (or Unknown)

License: [Licence agreement concerning inclusion of doctoral thesis in the Institutional Repository of the University of Leiden](#)

Downloaded from: <https://hdl.handle.net/1887/48284>

**Note:** To cite this publication please use the final published version (if applicable).

Cover Page



Universiteit Leiden



The handle <http://hdl.handle.net/1887/48284> holds various files of this Leiden University dissertation

**Author:** Baggelaar, M.P.

**Title:** Activity-based protein profiling of diacylglycerol lipases

**Issue Date:** 2017-04-06

# CHAPTER 7

## Focused Library Screening Using Activity-based Probes Reveals Novel Inhibitors of the $\alpha,\beta$ -hydrolase Fold Family\*

### Introduction

The activity-based probes (ABPs) MB064 and MB108 that were initially designed to target diacylglycerol lipase- $\alpha$  are non-specific ABPs that label multiple enzymes. After a close look at their target profiles in chapter 3, 4 and 6 it became apparent that they showed affinity for multiple  $\alpha,\beta$ -hydrolase fold domain (ABHD) containing proteins. These targets included ABHD6, ABHD12 and ABHD16a, therefore it was hypothesized that MB064 and MB108 could potentially serve as broad-spectrum ABPs for the  $\alpha,\beta$ -hydrolase fold protein superfamily.

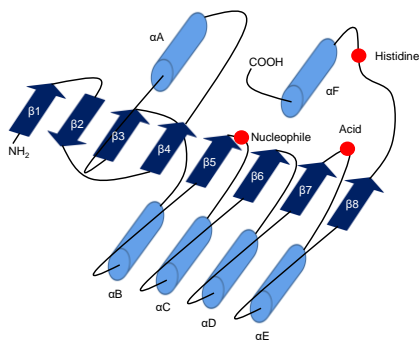


**Figure 1.** Structure of the  $\alpha,\beta$ -hydrolase fold. B-sheets are denoted as arrows and  $\alpha$ -helices are denoted as cylinders. The amino acids of the catalytic triad are depicted in red. Figure is adapted from Nardini and Dijkstra.<sup>1</sup>

The  $\alpha,\beta$ -hydrolase protein fold was discovered 1992 by Ollis *et al.*<sup>2</sup> This protein family is one of the largest and most diverse protein families, covering most, albeit not all, serine hydrolases. The  $\alpha,\beta$ -hydrolase fold family includes lipases, esterases, epoxidases, peroxide hydrolases and dehalogenases.<sup>2</sup> The  $\alpha,\beta$ -fold is characterized by 8  $\beta$ -strands forming a central  $\beta$ -sheet, which is surrounded and

\*Xavier Ruf and Hans den Dulk are kindly acknowledged for the generation of the ABHD constructs and Bogdan I. Florea is kindly acknowledged for the analysis of proteomics samples.

connected by 6  $\alpha$ -helices and several loops (Figure 1).<sup>1</sup> A catalytic triad formed by a catalytic nucleophile, an acidic residue and a histidine is responsible for hydrolase activity. The catalytic nucleophile resides within the nucleophilic elbow, which can be recognized by the consensus motif Sm-X-Nu-X-Sm (Sm = small residue, X = any residue, Nu = nucleophile). A special subgroup of the  $\alpha,\beta$ -hydrolase family are the ABHD proteins, which consists of 22 members. Members sharing the ABHD nomenclature generally have a GXSSXG motif.<sup>3</sup> Conserved structural features shared by this subfamily predict common roles in lipid biosynthesis and metabolism.<sup>3</sup> Dysregulated lipid metabolism is the underlying cause of many human disorders.<sup>4,5</sup> Despite their potentially important roles in pathological conditions, products and substrates of the ABHD family members and their position in lipid metabolic pathways are largely unknown.

ABHD family members play important roles in various (patho)physiological processes. For example,  $\alpha,\beta$ -hydrolase domain-containing protein 2 (ABHD2) is essential in hepatitis B virus propagation,<sup>6</sup> and has recently been identified as an enzyme that stimulates sperm activation.<sup>7</sup> ABHD11 is deleted in the Williams-Beuren syndrome,<sup>8</sup> and mutations in ABHD12 have been shown to be causative in polyneuropathy, hearing loss, ataxia, retinitis pigmentosa and cataract (PHARC).<sup>9</sup> The physiological role of many members of this enzyme family is not elucidated. Small molecule inhibitors for these enzymes are likely to provide valuable information on the (patho)physiological functions of these enzymes, and may potentially serve as leads for novel therapeutic agents.

In this chapter ABPs MB108 and MB064 are profiled as broad-spectrum probes for the  $\alpha,\beta$ -hydrolase fold protein family. Broad-spectrum probes are unique in their ability to enable screening of an inhibitor library against multiple enzymes in parallel. A library against library screen of 7 enzymes against 200+ inhibitors facilitated rapid identification of inhibitors for ABHD2 and ABHD3. No inhibitors are currently available for these enzymes. It is anticipated that these new inhibitors will be instrumental to study the (patho)physiological role of ABHD2 and ABHD3.

## Results

### Identification of $\alpha,\beta$ -hydrolase fold containing proteins targeted by MB064 and MB108

A large variety in expression for  $\alpha,\beta$ -hydrolase fold family members across different tissue types has been observed by *in-situ* hybridization and in global proteomics studies.<sup>3,10-12</sup> Therefore, it was investigated whether this tissue specific expression was mirrored in the enzyme activity measured by ABP MB064. The labeling profile of fluorescent ABP MB064 in the mouse cytosol and membrane fractions of the brain, heart, kidney, liver, lung, pancreas, spleen and testes was examined (Figure 2B). A highly diverse labeling pattern across different tissue types was observed, in particular in the membrane fraction. Therefore, the extent of  $\alpha,\beta$ -hydrolase fold family members targeted by a biotinylated

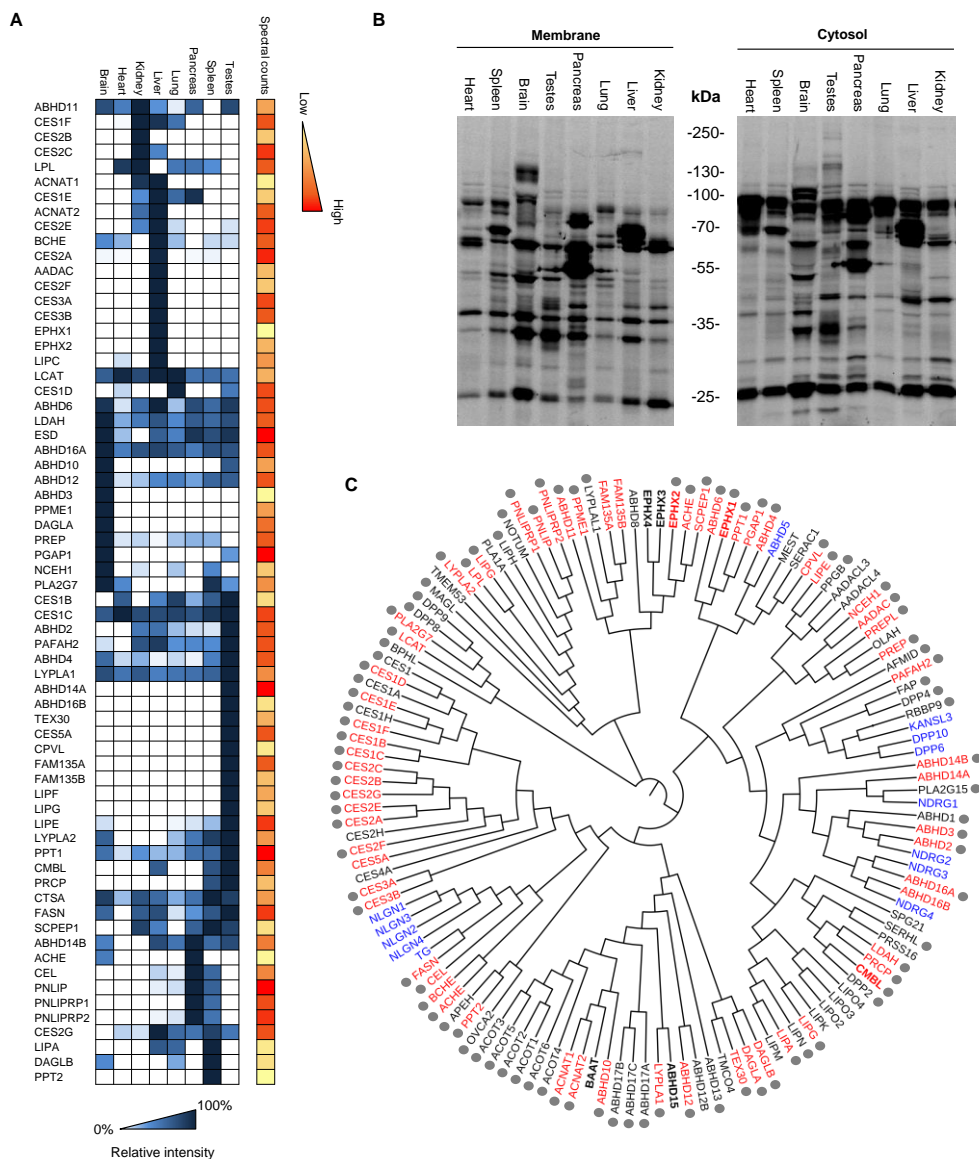


**Figure 2.** Detection of  $\alpha,\beta$ -hydrolase fold enzyme activity in the mouse brain proteome using  $\beta$ -lactone based ABPs MB064 and MB108. (A) Chemoproteomic screen of  $\alpha,\beta$  hydrolase fold enzyme activity in the mouse proteome using  $\beta$ -lactone based activity-based probe MB108 (10  $\mu$ M). Mean of the average spectral counts over three replicate experiments. Heatmap: proteins are ordered by hierarchical clustering. Intensity in blue represents the relative activity per protein in each tissue. Intensity in orange are the spectral counts in the tissue where the protein shows highest activity. (B) Gel based tissue screen with ABP MB064 (2  $\mu$ M) in the membrane and cytosolic mouse proteome. (C) Phylogenetic tree of  $\alpha,\beta$ -hydrolase fold proteins generated by multiple sequence alignment (Muscle) and ClustalW2 omega phylogeny.<sup>14</sup> Proteins highlighted in red are targeted by MB108. All proteins are serine hydrolases except those in bold or highlighted in blue. Blue proteins lack a catalytic residue.

Bold proteins have a cysteine or asparagine as a catalytic residue. Grey dots indicate organophosphate targeted proteins.<sup>10,15</sup>

version of MB064 (MB108) was comprehensively determined in a tissue-wide chemoproteomic screen. MB108 contains the same warhead and recognition element as MB064 and is therefore expected to have a similar target profile.

As a reference for probe targets, a list of  $\alpha,\beta$ -hydrolase fold enzymes was retrieved from the ESTHER database (<http://bioweb.ensam.inra.fr/esther>), which is widely used to monitor proteins containing a  $\alpha,\beta$ -hydrolase fold.<sup>13</sup> 136 mouse  $\alpha,\beta$ -hydrolase fold containing proteins were retrieved from the database. The sequences of the  $\alpha,\beta$ -hydrolase fold containing proteins were aligned and a phylogenetic tree was generated using multiple sequence alignment (Muscle) and ClustalW2 omega phylogeny (Figure 2C).<sup>14</sup> The  $\alpha,\beta$ -hydrolase fold containing proteins detected in in the chemoproteomic screen which were  $>5$  fold enriched (quantification based on spectral counts) compared to heat denaturated controls are highlighted in red. The screen revealed that 66 out of the 136 mouse  $\alpha,\beta$ -hydrolase fold proteins were detected by MB108 in one or more tissues (Figure 2A). In addition, a number of hydrolases and transferases that did not contain the  $\alpha,\beta$ -hydrolase fold motif, but have a catalytic nucleophile that can attack the  $\beta$ -lactone were also targeted. These proteins are given in Supporting Figure 1.

It is well-known that  $\alpha,\beta$ -hydrolase fold proteins react well with organophosphates.<sup>15</sup> Therefore, organophosphate-based ABPs are suitable tools to study  $\alpha,\beta$ -hydrolase fold enzymatic activity. Bachovchin *et al.* have targeted  $>80\%$  of mammalian metabolic serine hydrolases using a single fluorophosphonate-based ABP.<sup>10</sup> Proteins that are known to interact with organophosphates are marked with a grey dot in Figure 1C. A large overlap between the targets of the organophosphates and MB108 was observed. Importantly, MB108 targeted FAM135, FAM135B, CES5A and ABHD14A, which are not targeted by organophosphate-based probes.<sup>10,15</sup>

In conclusion, the  $\beta$ -lactone based ABPs, MB108 and its fluorescent analogue MB064 are broad-spectrum ABPs. They are highly versatile and powerful tools to study the activity of many ( $\sim 50\%$ ) of the members of the  $\alpha,\beta$ -hydrolase fold family, including several members that are not detected by organophosphate-based probes.

### **Gel-based assay for identification $\alpha,\beta$ -hydrolase family**

The biochemical and physiological functions of many members of the  $\alpha,\beta$ -hydrolase fold family are not known and selective small molecule inhibitors for members of this family are scarce. Inhibitors that enable spatiotemporal control over enzyme activity are highly valuable tools to elucidate enzyme function. The  $\alpha,\beta$ -hydrolase fold subfamily sharing the ABHD nomenclature share conserved structural motifs that suggest common roles in lipid metabolism.<sup>3</sup> Therefore, a competitive screen between ABHD proteins and a targeted lipase

inhibitor library was envisioned to identify novel modulators for members of this subfamily.

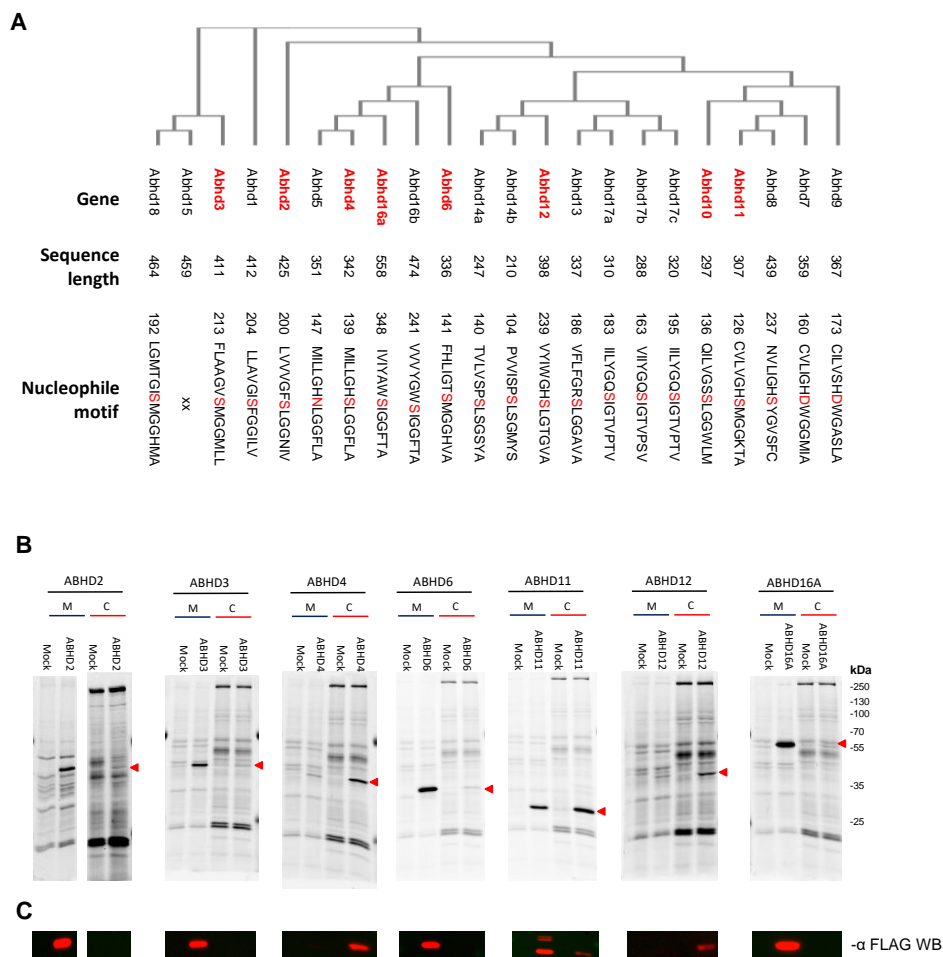


**Figure 3.** (A) phylogenetic tree of the  $\alpha,\beta$ -hydrolase fold family members sharing the ABHD nomenclature. The tree is generated by multiple sequence alignment (Muscle) and ClustalW2 omega phylogeny.<sup>14</sup> Proteins used for the inhibitor screen are highlighted in red. (B) Labeling of ABHD proteins overexpressed in HEK293T or U2OS cells. Protein labeling of ABHD transfected cells was compared to mock transfected cells in the membrane (M) and cytosolic (C) fractions. Proteins (1 mg/mL) were labeled by ABP MB064 (2  $\mu$ M). Overexpressed proteins are marked by a red triangle. (C) Anti-FLAG western blot for confirmation of protein expression and localization of the transfected ABHD. Cutout at the molecular weight indicated by the red triangle is represented.

Chemoproteomic ABPP is highly sensitive and allows the study of native enzymes with relative low abundance and activity in tissues or cell lines. However, chemoproteomics is costly and time consuming, thus not suitable for high throughput screening of inhibitor

libraries. Therefore, a gel-based assay using the fluorescent analogue of MB108, MB064 was employed to identify novel inhibitors for ABHD family members. A gel-based assay is compatible with screening of a considerable number of inhibitors (200+) against multiple enzymes at the same time in one assay. It is important to note that it is challenging to correlate enzymes to specific fluorescent bands on SDS-PAGE in native proteomes. Native enzymes show large variations in labeling intensities and display unequal tissue distribution. Therefore, it is difficult to make a generic assay for multiple proteins of interest in native proteome. Recombinant expression of proteins avoids several of these problems and is highly suitable for generating custom protein libraries for inhibitor screening.

The human enzymes sharing the ABHD nomenclature corresponding to the enzymes that were detected in the chemoproteomic mouse tissue screen were recombinantly expressed in HEK293T or U2OS cells (Figure 3A). The constructs were equipped with a FLAG tag to monitor protein expression and gel migration. Human ABHD3, 4, 6, 11, 12 and 16A were recombinantly expressed in HEK293T cells. ABHD2 was expressed in U2OS cells because the efficiency of overexpression for ABHD2 in HEK293T cells was low. No expression of ABHD10, 14A, 14B and 16B in HEK293T nor U2OS could be achieved for reasons that are not completely understood. Labeling (ABP MB064 (2  $\mu$ M)) of lysates from transfected cells and comparison to mock transfected cells was used to monitor protein activity. ABHD2, 3, 6, and 16A showed the highest activity in the membrane fraction, ABHD4 and 12 in the cytosolic fraction and ABHD11 showed high labeling efficiencies in both cytosolic and membrane fractions, with a slightly higher signal in the cytosol.

To establish a multiple protein assay, recombinantly expressed proteins were pooled in custom made protein libraries. ABHD3, 4 and 12 are clustered around a molecular weight of ~40 kD. Therefore, two protein libraries were required resolve all expressed ABHDs on 1D SDS-PAGE. Protein library 1 contained ABHD2, 3 and 12, and protein library 2 consists of ABHD4, 6, 11 and 16A.

The lipase-focused library contained 207 inhibitors, and was divided in three major classes ( $\alpha$ -ketoamides,  $\beta$ -ketoamides and 1,2,4-triazole ureas) and a set of unique chemotypes (singletons). The compound library was screened at 10  $\mu$ M against the two protein libraries, resulting in the rapid generation of ~1500 protein-inhibitor interaction data points. The screen revealed that all proteins were hit by one or more compounds (Figure 4D). Inhibitors were qualified as a hit when protein labeling was reduced > 70% compared to vehicle-treated control. A clear distinction between target profiles of different inhibitor classes was detected (Figure 4E). The  $\alpha$ -ketoamides were practically inactive against all tested ABHD family members. The  $\beta$ -ketoamides provided an excellent chemotype to inhibit ABHD3; 21 hits were identified of which 13 compounds were considered selective (< 50% inhibition of the other ABHDs). Compound **47** and **60** were the most potent inhibitors that remained selective over the other measured ABHDs. Inhibitors from the 1,2,4 triazole-urea class were more reactive. This class effectively targeted ABHD6 and

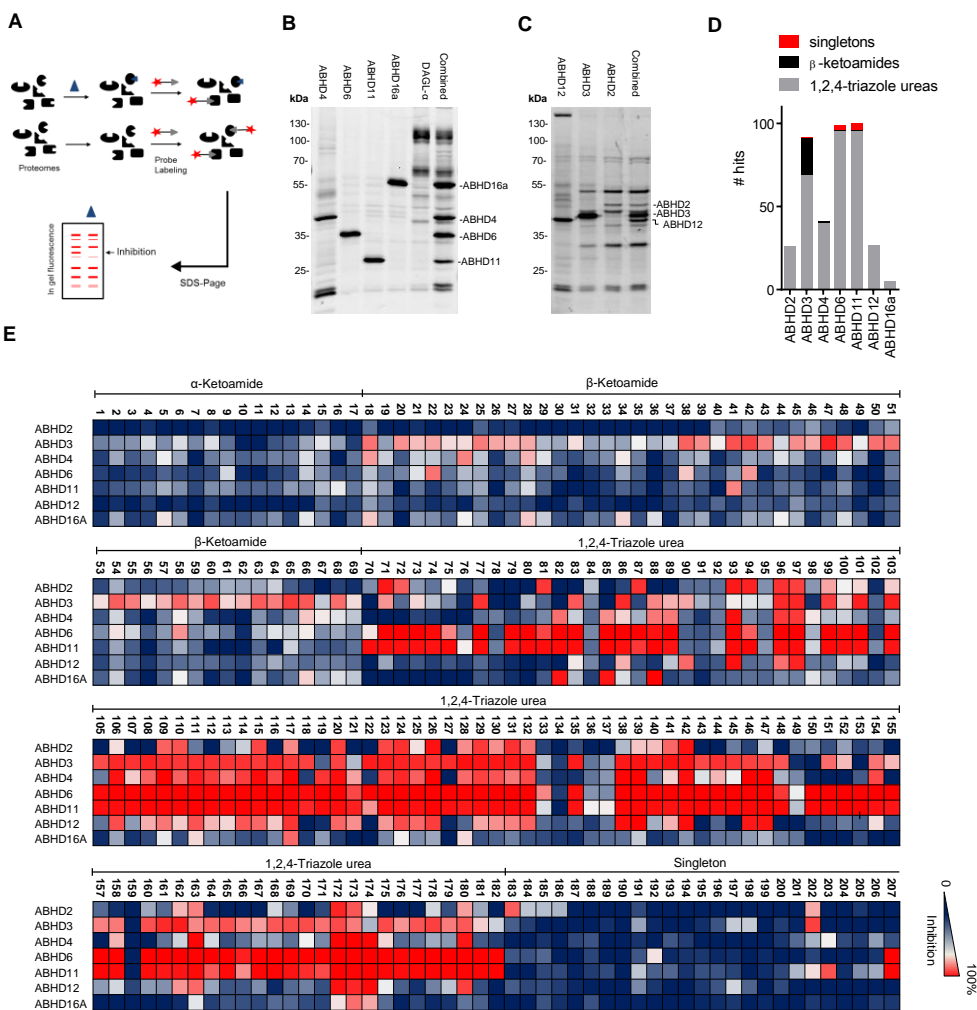


**Figure 4.** (A) Schematic representation of the gel-based competitive ABPP workflow. (B). Fluorescent labeling (MB064, 2  $\mu$ M) of HEK293T lysates that overexpress ABHD4, 6, 11, 16A and DAGL- $\alpha$ , and a combination thereof to form protein library 1. (C) Fluorescent labeling (MB064, 2  $\mu$ M) of HEK293T lysates that overexpress ABHD12, 3, 2 and a combination thereof to form protein library 2. (D) Graphical representation of the number of hits per chemotype per enzyme. (E) Heatmap overview of the inhibitor screen.

ABHD11, >70% of the 1,2,4-triazole ureas were classified as hits for these enzymes. Compound **183** from the singleton series reduced labeling of ABHD2 with more than 70% without reducing labeling of other ABHDs with more than 50%. No selective inhibitors were found for ABHD4, 6, 11, 12, or 16A, but the non-selective compounds may still represent interesting starting points for hit optimization programs. Since no selective

inhibitors are known for ABHD2 and ABHD3, it was decided to analyze compounds **183**, **47** and **60** in more detail.

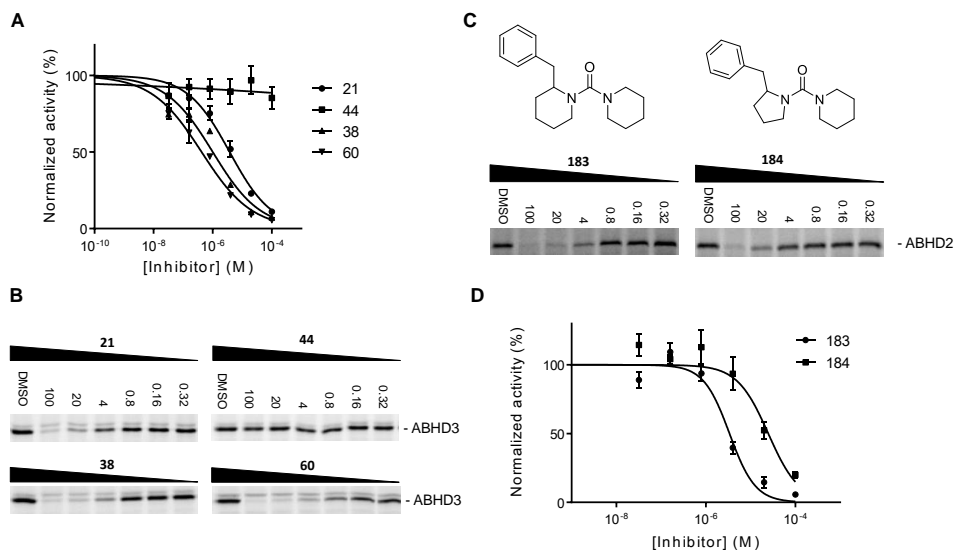
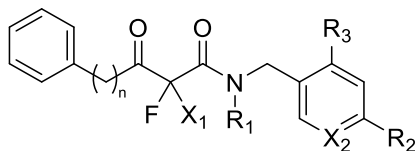


**Figure 5.** Structure activity of lead inhibitors for ABHD2 and ABHD3. (A) Dose response curves of inhibitor **21**, **44**, **38**, **60**. (B) Dose dependent inhibition of MB064 (2 μM) of ABHD3 by inhibitor **1**, **5**, **8** and **9** on gel. (C) Dose dependent inhibition of MB064 (2 μM) labeling of ABHD2 on gel. (D) Dose response curve of inhibitor **183**  $pIC_{50} = 5.5 \pm 0.06$  ( $n = 3$ ;  $\pm$ SEM) and **184**  $pIC_{50} = 4.6 \pm 0.1$  ( $n = 3$ ;  $\pm$ SEM). All experiments were performed in triplicate.

**Table 1.** SAR of  $\beta$ -ketoamides against ABHD3.



Entry*	n	X <sub>1</sub>	X <sub>2</sub>	R <sub>1</sub>	R <sub>2</sub>	R <sub>3</sub>	pIC <sub>50</sub>
<b>21</b>	2	F	C	H	H	H	5.42 ± 0.07
<b>39<sup>a</sup></b>	2	F	C	H	H	H	5.36 ± 0.08 <sup>a</sup>
<b>24</b>	1	F	C	H	H	H	N/A
<b>23</b>	2	H	C	H	H	H	N/A
<b>44</b>	2	F	C	Me	H	H	N/A
<b>47</b>	2	F	N	H	H	H	5.64 ± 0.10
<b>53</b>	2	F	C	H	H	CF <sub>3</sub>	4.42 ± 0.22
<b>38</b>	2	F	C	H	F	H	6.00 ± 0.08
<b>60</b>	2	F	C	H	OMe	F	6.38 ± 0.06

<sup>a</sup> $\beta$ -ketone reduced to an alcohol. <sup>\*</sup>dilute  $\beta$ -ketoamides show two peaks on LC/MS, which is hypothesized to be caused by hydration of the ketone.

Compound **183** was found to inhibit ABHD2 with a  $\text{pIC}_{50}$  of  $5.5 \pm 0.06$  (Figure 5C, D). The structurally related compound **184**, which contains a pyrrolidine instead of a piperidine, showed a 10-fold drop in activity with a  $\text{pIC}_{50}$  of  $4.6 \pm 0.1$ .

To investigate the structure activity relationship of  $\beta$ -keto heterocycles against ABHD3, a dose-response analysis on a selected subset of the  $\beta$ -keto heterocycles identified in the focused library screen was performed. The two most potent selective inhibitors **47** and **60** and structural analogues which could provide important information on the SAR were selected for a more detailed analysis (Table 1). Compound **21** represents the core structure of most active  $\beta$ -keto heterocyclic ABHD3 inhibitors, and had a  $\text{pIC}_{50}$  of  $5.4 \pm 0.07$ . Remarkably, compound **39**, where the  $\beta$ -ketone of **21** was replaced by an alcohol was also active on ABHD3. A methyl spacer instead of an ethyl spacer between the  $\beta$ -ketone and phenyl group **24** was not allowed. Compound **44**, which contains an N-methylated amide was inactive and compound **23** which has a hydrogen instead of a fluorine at  $X_1$  was also inactive. The inhibitor where the eastern phenyl group was replaced by a pyridine **47** has a  $\text{pIC}_{50}$  of  $5.64 \pm 0.10$ . A  $\text{CF}_3$  group on the *ortho* position of the eastern phenyl group **53** showed 10-fold less activity compared to **47**. Compound **38** showed considerable activity with a  $\text{pIC}_{50}$  of  $6.00 \pm 0.08$ , but the inhibitor with an *o*-fluoro-*p*-methoxyphenyl substituent on the eastern side **60** was the most potent inhibitor, with a  $\text{pIC}_{50}$  of  $6.38 \pm 0.06$ . Therefore, compound **60** was selected for a selectivity assessment.

### Inhibitor selectivity

To investigate the selectivity of inhibitors **60** and **150** in native mouse proteome, comparative and competitive ABPP with broad-spectrum FP-based probes (TAMRA-FP and FP-biotin) and the ABPs MB064 and MB108 was employed (Figure 6).<sup>16</sup> The fluorophosphonate was added to broaden the scope of the selectivity profile because it is known to target many serine hydrolases.<sup>10</sup> Since, ABHD3 was only detected in the brain (Figure 1A), the selectivity of compound **60** was tested in this tissue. Gel-based competitive ABPP revealed that **60** (20  $\mu\text{M}$ , 30 min) reduced labeling of a band at  $\sim 35$  kD in the membrane fractions using both ABPs. This band has previously been identified as ABHD6. The identity of the off-target was confirmed by a competitive chemoproteomic assay with FP-biotin.<sup>16-18</sup>

The selectivity of ABHD2 inhibitor **183** (20  $\mu\text{M}$ , 30 min) was investigated in mouse testes. Compound **183** reduced labeling of two fluorescent bands in the membrane proteome as determined by MB064. The competitive chemoproteomic assay confirmed ABHD2 inhibition, but no other targets were detected. Together these studies indicate that inhibitor **183** shows a highly selective labeling profile and can be used to inhibit ABHD2 in the testes proteome in an acute fashion with high selectivity.

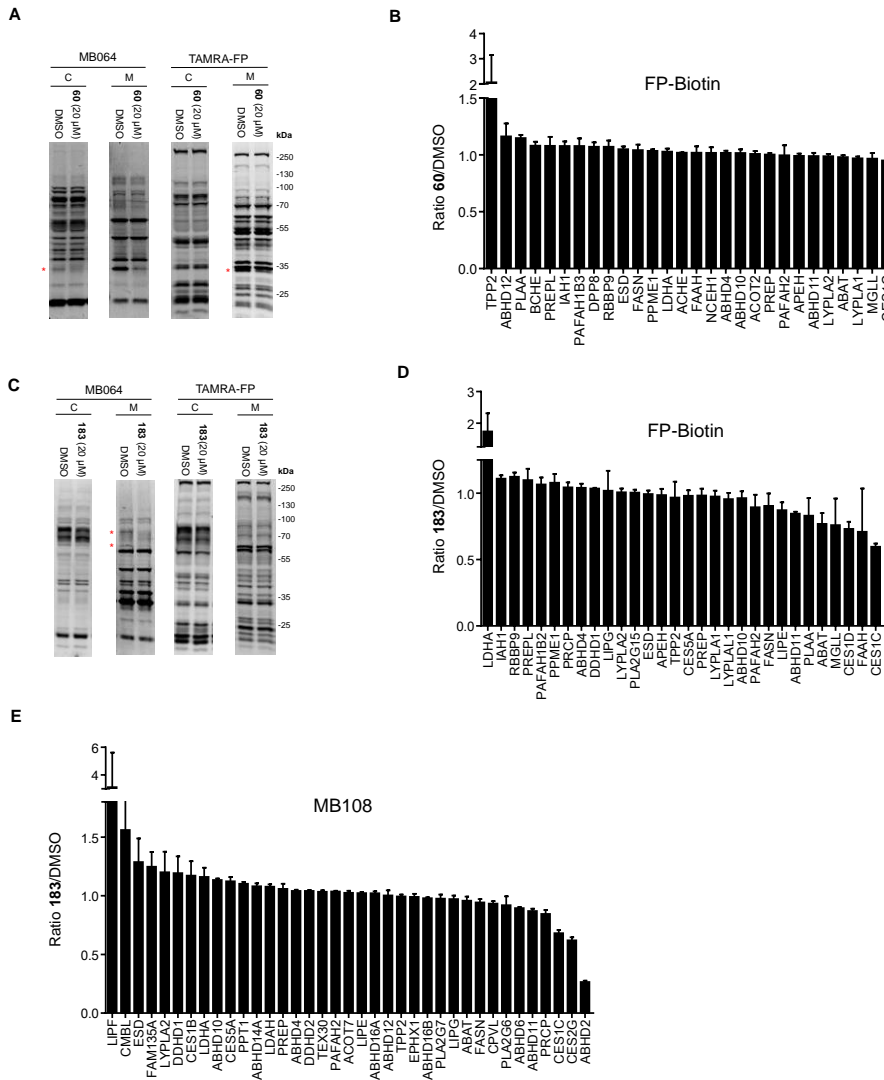


**Figure 6.** Selectivity of identified inhibitors for ABHD2 and ABHD3. (A) Gel-based competitive ABPP with inhibitor **60** (20  $\mu$ M) against TAMRA FP (2  $\mu$ M) and MB064 (2  $\mu$ M) in the brain cytosolic and membrane fractions (n=3). (B) Competitive chemoproteomic selectivity assay of inhibitor **60** (20  $\mu$ M) in the mouse brain proteome using ABP FP-biotin (10  $\mu$ M; n=3). (C) Gel-based competitive ABPP with inhibitor **183** (20  $\mu$ M) against TAMRA-FP (2  $\mu$ M) and MB064 (2  $\mu$ M) in the mouse testes cytosolic and membrane fractions (n =3). (D) Competitive chemoproteomic selectivity assay of inhibitor **183** (20  $\mu$ M) in the testes proteome using ABP FP-biotin (10  $\mu$ M' n=3). (E) Competitive chemoproteomic selectivity assay of inhibitor **183** (20  $\mu$ M) in the mouse testes proteome using ABP MB108 (10  $\mu$ M; n=3).

## Discussion/Conclusion

The target profile of ABP MB108 and MB064 across the mouse proteome (spleen, pancreas, liver, testes, brain, kidney, heart and lung) was mapped. This revealed MB108 and MB064 as highly suitable broad spectrum ABPs to study the activity of  $\alpha,\beta$ -hydrolase fold proteins. The ABPs target ~50% of the  $\alpha,\beta$ -hydrolase fold superfamily, including FAM135A, FAM135B, ABHD14B and CES5A, which are not detected by organophosphates.<sup>10</sup> This remarkably nonspecific target profile demonstrates that it is important to look at the full target profile of an ABP to make optimal use of its properties. The value of MB108 and MB064 as tools for the identification of inhibitors for  $\alpha,\beta$ -hydrolase fold family members was shown by the rapid identification of inhibitors for ABHD2, (**183**) and ABHD3, (**60**).

The biochemical role of ABHD3 has been examined by untargeted metabolomics in ABHD3 knockout mice.<sup>19</sup> ABHD3 is a medium chain ( $C_{14}$ ) phosphatidylcholine (PC) phospholipase and its genetic deletion elevates  $C_{14/18:2}$ -PC,  $C_{14/20:4}$ -PC and  $C_{14:22:6}$ -PC. In addition, ABHD3 also cleaves phosphatidylcholines (PCs) with shorter acyl chains and oxidatively truncated PCs (oxPCs). These oxPCs are involved in the promotion of cell death and atherosclerosis.<sup>20,21</sup> Inhibitors can be used to study the effect of acute modulation of ABHD3 activity and its medium chain phospholipid substrates in physiological processes where these lipids have been postulated to be involved in a range of signaling functions.<sup>22,23</sup>

ABHD2 plays an important role in hepatitis B virus propagation and may serve as a novel drug target for anti-hepatitis-B drug development.<sup>6</sup> ABHD2 is also associated with chronic diseases that involve monocyte/macrophage recruitment, such as emphysema and atherosclerosis.<sup>24-26</sup> Recently, 2-AG was identified as a substrate for ABHD2.<sup>7</sup> The enzyme is highly expressed in spermatozoa and acts as a progesterone-dependent hydrolase. 2-AG inhibits the sperm calcium channel CatSper. 2-AG hydrolysis by ABHD2 leads to calcium influx and sperm activation. Therefore, ABHD2 could be an interesting target for the development of male contraceptives.

The ABHD2 and ABHD3 inhibitors **183** and **60** respectively are likely to become useful tools to study the biological role of ABHD2 and ABHD3. Furthermore they provide excellent leads for further development toward more potent and more selective inhibitors for these enzymes.

## Experimental methods

**Cell culture.** Cell culture was performed as described in chapter 3 and 4. In brief, HEK293T or U2OS cells were grown in DMEM with stable glutamine and phenolred (PAA), 10% New Born Calf serum, penicillin and streptomycin. Cell passage was performed every 2-3 days by resuspension in medium and seeding to appropriate confluence.

**Transfection and cell lysis.** 24h prior to transfection  $10^7$  cells were seeded in a 15 cm petri dish. A 3:1 mixture of polyethyleneimine (60 $\mu$ g) and plasmid DNA (20 $\mu$ g) in 2 mL serum free medium was added. The medium was refreshed after 24 hours, and after 72h HEK293T (48h for U2OS) cells were harvested in 20 mL medium. Cells were isolated by centrifugation for 10 min at 1000 rpm and subsequent aspiration of the medium. The cell pellet was flash frozen in liquid nitrogen and stored at -80 °C until use.

Cell pellets were slowly thawed on ice and suspended in lysis buffer (20 mM HEPES pH 7.2, 2 mM DTT, 0.25 M sucrose, 1 mM MgCl<sub>2</sub>, 25 U/mL Benzonase). Three pulses with a polytrone (3  $\times$  7 sec) were used to homogenize the suspension. After homogenization, the suspension was allowed to incubate for 10 min on ice. Ultracentrifugation (100.000  $\times$  g, 45 min, 4 °C, Beckman Coulter, Type Ti70 rotor) was used to separate the cytosolic and membrane fraction. The pellet (membrane fraction) was resuspended in storage buffer (20 mM HEPES pH 7.2, 2 mM DTT). The total protein concentration was determined with Quick Start Bradford assay (Biorad) or Qubit<sup>TM</sup> protein assay (Invitrogen). The lysates were flash frozen in liquid nitrogen and stored at -80 °C until use.

**Preparation of mouse tissue proteome.** Mouse tissue were isolated according to guidelines approved by the ethical committee of Leiden University (DEC#13191). Mouse tissues were dounce homogenized in pH 7.2 lysis buffer A (20 mM HEPES pH 7.2, 2 mM DTT, 1 mM MgCl<sub>2</sub>, 25 U/mL Benzonase) and incubated for 5 minutes on ice. The suspension was centrifuged (2500  $\times$  g, 3 min, 4 °C) to remove debris. The supernatant was collected and subjected to ultracentrifugation (100.000  $\times$  g, 45 min, 4 °C, Beckman Coulter, Type Ti70 rotor). This yielded the membrane fraction as a pellet and the cytosolic fraction in the supernatant. The membrane fraction was suspended in storage buffer (20 mM HEPES pH 7.2, 2 mM DTT). The total protein concentration was determined with Quick Start Bradford assay (Biorad) or Qubit<sup>TM</sup> protein assay (Invitrogen). Membranes and supernatant were flash frozen in liquid nitrogen and stored in aliquots at -80 °C until use.

**Gel-based tissue screen (MB064):** The membrane or lysate fraction of mouse brain, heart, kidney, liver, lung, pancreas, spleen or testes was diluted to 1 mg/mL. Proteome (1 mg/mL, 20  $\mu$ L) was incubated at 37 °C for 15 min with MB064 (1  $\mu$ M, final concentration). After 15 min the reactions were quenched with 10  $\mu$ L standard 3  $\times$  SDS-PAGE sample buffer.

The samples were directly loaded and resolved on SDS PAGE gel (10 % acrylamide). The gels were scanned using a ChemiDoc MP system (Cy3 settings, 605/50 filter) and analyzed using Image lab 4.1.

**Chemoproteomic tissue screen.** The membrane or lysate fraction of mouse brain, heart, kidney, liver, lung, pancreas, spleen or testes was diluted to 2 mg/mL. The proteomes (490  $\mu$ L) were incubated with 10  $\mu$ L 500  $\mu$ M ABP MB108 (final concentration 10  $\mu$ M) for 1h at rt. The labeling reaction was quenched and excess probe was removed by chloroform methanol precipitation. Precipitated proteome was suspended in 500  $\mu$ L 6M Urea/25 mM ammonium bicarbonate and allowed to incubate for 15 minutes. 5  $\mu$ L (1 M DTT) was added and the mixture was heated to 65 °C for 15 minutes. The sample was allowed to cool to rt before 40  $\mu$ L (0.5 M) iodoacetamide was added and the sample was alkylated for 30 minutes in the dark. 140  $\mu$ L 10% (wt/vol) SDS was added and the proteome was heated for 5 minutes at 65 °C. The sample was diluted with 6 mL PBS. 100  $\mu$ L of 50% slurry of Avidin–Agarose from egg white (Sigma-Aldrich) was washed with PBS and added to the proteome sample. The beads were incubated with the proteome for 3h.

Beads were isolated by centrifugation and washed with 0.5% (wt/vol) SDS and PBS (3x). The proteins were digested overnight with sequencing grade trypsin (Promega) in 100  $\mu$ L Pd buffer (100 mM Tris Ph 7.0, 100 mM NaCl, 1 mM CaCl<sub>2</sub>, 2 % ACN and 500 ng trypsin) at 37 °C with vigorous shaking. The pH was adjusted with formic acid to pH 3 and the beads were removed. The samples were further purified and measured as described in chapter 3.

**Enzyme mixes for inhibitor screen.** Protein library 1 is made in standard assay buffer (20 mM HEPES pH 7.2, 2 mM DTT) and contains the following transiently transfected proteins (concentrations are final concentrations). 4 mg/mL cytosolic fraction of ABHD12 transfected HEK293T cell lysate, 0.3 mg/mL membrane fraction ABHD3 transfected HEK293T cell lysate, and 1 mg/mL membrane fraction of ABHD2 transfected U2OS cell lysate.

Protein library 2 is made in standard assay buffer (20 mM HEPES pH 7.2, 2 mM DTT) and contains the following transiently transfected proteins (concentrations are final concentrations). 1 mg/mL cytosolic fraction of ABHD4 transfected HEK293T cell lysate, 0.25 mg/mL membrane fraction ABHD6 and 11 transfected HEK293T cell lysate, 0.2 mg/mL membrane fraction ABHD16A transfected HEK293T cell lysate and finally 0.5 mg/mL membrane fraction DAGL- $\alpha$  transfected HEK293T cell lysate.

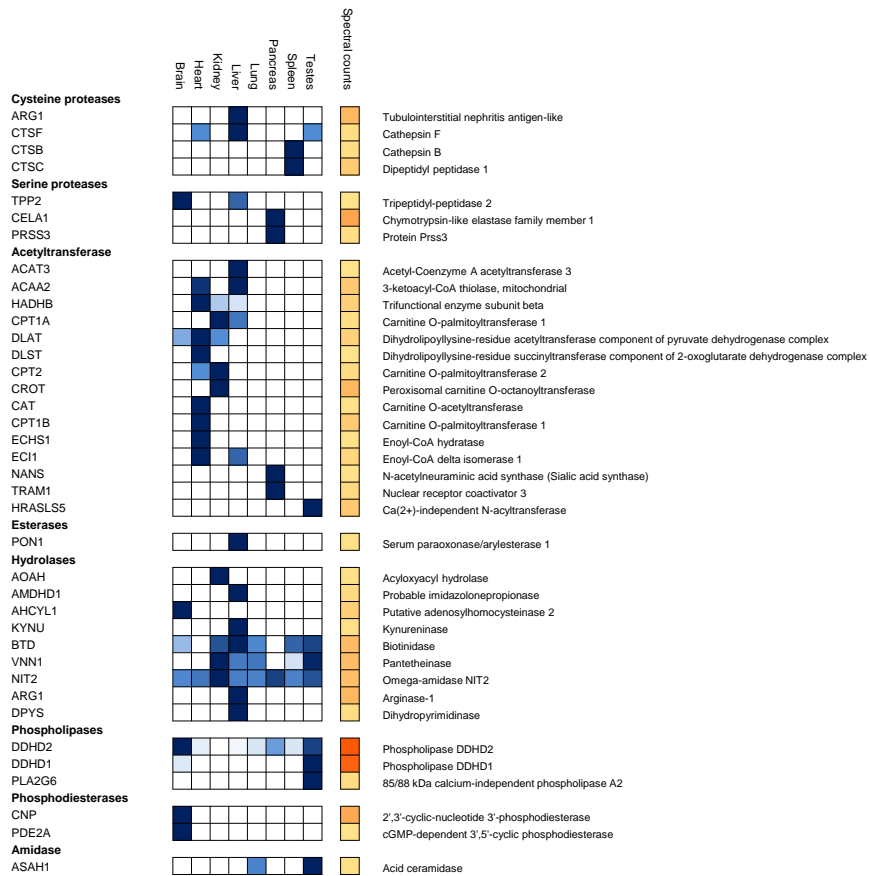
**Inhibitor screen.** Enzyme mix 1 or 2 (19.5  $\mu$ L) was incubated with DMSO (0.5  $\mu$ L) or inhibitor (0.5  $\mu$ L, 400  $\mu$ M; 10  $\mu$ M final concentration) for 30 min at 37 °C. Next MB064 (0.5  $\mu$ L, 80  $\mu$ M; 2  $\mu$ M final concentration) was incubated for 15 min at 37 °C. The reactions were quenched with 10  $\mu$ L standard 3  $\times$  SDS PAGE sample buffer. The samples

were directly loaded and resolved on SDS PAGE gel (10 % acrylamide). The gels were scanned using a ChemiDoc MP system (Cy3 settings, 605/50 filter) and the percentage inhibition was determined by comparison with DMSO (100%) using Image lab 4.1. Control for protein loading was performed by coomassie staining and adjustment for total lane intensity.

**Gel-based dose-response analysis.** Dose response analysis was performed as described in chapter 4. In brief, transfected proteome (19.5  $\mu$ L) was incubated with DMSO (0.5  $\mu$ L) or inhibitor (0.5  $\mu$ L) at indicated final concentrations for 30 min at 37 °C. Next MB064 (0.5  $\mu$ L, 80  $\mu$ M; 2  $\mu$ M final concentration) was incubated for 15 min at 37 °C. The reactions were quenched with 10  $\mu$ L standard 3  $\times$  SDS PAGE sample buffer. The samples were directly loaded and resolved on SDS PAGE gel (10 % acrylamide). The gels were scanned using a ChemiDoc MP system (Cy3 settings, 605/50 filter) the percentage of activity remaining was determined by measuring the integrated optical intensity of the fluorescent protein bands using Image lab 4.1. The relative intensity was compared to the vehicle treated proteins, which were set to 100%. Correction for protein loading was performed by coomassie staining. IC50 values were determined by plotting log(inhibitor) vs. normalized response (variable slope) dose-response curve generated using Prism software (GraphPad).

**Selectivity in native mouse proteome.** The gel-based selectivity assay was performed in a similar fashion as described in chapter 4. In brief, mouse testes or brain cytosolic or membrane fractions were diluted to a total protein concentration of 2 mg/mL. Proteome (19.5  $\mu$ L) was incubated with DMSO (0.5  $\mu$ L) or inhibitor (0.5  $\mu$ L, 20  $\mu$ M final concentration) for 30 min at 37 °C. Next MB064 or TAMRA-FP (0.5  $\mu$ L, 80  $\mu$ M; 2  $\mu$ M final concentration) was incubated for 15 min at 37 °C. The reactions were quenched with 10  $\mu$ L standard 3  $\times$  SDS PAGE sample buffer and analysed as described in chapter 4.

**Chemoproteomic selectivity assay in native mouse proteome.** Mouse testes or brain cytosolic or membrane fraction was diluted to a total protein concentration of 2 mg/mL. 5  $\mu$ L 1 mM inhibitor (20  $\mu$ M final concentration) or DMSO was added to 240  $\mu$ L proteome and allowed to incubate for 30 min at 37 °C. FP-Biotin or MB108 (5  $\mu$ L, 500  $\mu$ M) was added and incubated for 30 min at 37 °C. The samples were further processed and analysed as described in chapter 4.



**Supporting figure 1.** Non  $\alpha,\beta$ -hydrolase fold proteins with hydrolase activity that were detected by MB108. Hydrolases, proteases, transferases, esterases and amidases as classified by panther gene ontology.

**References**

1. Nardini, M.; Dijkstra, B. W. *Curr. Opin. Struct. Biol.* **1999**, *9*, 732.
2. Ollis, D. L.; Cheah, E.; Cygler, M.; Dijkstra, B.; Frolow, F.; Franken, S. M.; Harel, M.; Remington, S. J.; Silman, I.; Schrag, J. *Protein Eng.* **1992**, *5*, 197.
3. Lord, C. C.; Thomas, G.; Brown, J. M. *Biochim. Biophys. Acta* **2013**, *1831*, 792.
4. Hotamisligil, G. S. *Nature* **2006**, *444*, 860.
5. Nomura, D. K.; Morrison, B. E.; Blankman, J. L.; Long, J. Z.; Kinsey, S. G.; Marcondes, M. C.; Ward, A. M.; Hahn, Y. K.; Lichtman, A. H.; Conti, B.; Cravatt, B. F. *Science* **2011**, *334*, 809.
6. Ding, X.; Yang, J.; Wang, S. *Oligonucleotides* **2011**, *21*, 77.
7. Miller, M. R.; Mannowetz, N.; Iavarone, A. T.; Safavi, R.; Gracheva, E. O.; Smith, J. F.; Hill, R. Z.; Bautista, D. M.; Kirichok, Y.; Lishko, P. V. *Science* **2016**, *352*, 555.
8. Merla, G.; Ucla, C.; Guipponi, M.; Reymond, A. *Hum. Genet.* **2002**, *110*, 429.
9. Fiskerstrand, T.; H'Mida-Ben Brahim, D.; Johansson, S.; M'Zahem, A.; Haukanes, B. I.; Drouot, N.; Zimmermann, J.; Cole, A. J.; Vedeler, C.; Bredrup, C.; Assoum, M.; Tazir, M.; Klockgether, T.; Hamri, A.; Steen, V. M.; Boman, H.; Bindoff, L. A.; Koenig, M.; Knappskog, P. M. *The Am. J. Hum. Genet.* **2010**, *87*, 410.
10. Bachovchin, D. A.; Ji, T.; Li, W.; Simon, G. M.; Blankman, J. L.; Adibekian, A.; Hoover, H.; Niessen, S.; Cravatt, B. F. *Proc. Natl. Acad. Sci. U. S. A.* **2010**, *107*, 20941.
11. Sharma, K.; Schmitt, S.; Bergner, C. G.; Tyanova, S.; Kannaiyan, N.; Manrique-Hoyos, N.; Kongi, K.; Cantuti, L.; Hanisch, U. K.; Philips, M. A.; Rossner, M. J.; Mann, M.; Simons, M. *Nat. Neurosci.* **2015**, *18*, 1819.
12. Uhlen, M.; Fagerberg, L.; Hallstrom, B. M.; Lindskog, C.; Oksvold, P.; Mardinoglu, A.; Sivertsson, A.; Kampf, C.; Sjostedt, E.; Asplund, A.; Olsson, I.; Edlund, K.; Lundberg, E.; Navani, S.; Szgyarto, C. A.; Odeberg, J.; Djureinovic, D.; Takanen, J. O.; Hober, S.; Alm, T.; Edqvist, P. H.; Berling, H.; Tegel, H.; Mulder, J.; Rockberg, J.; Nilsson, P.; Schwenk, J. M.; Hamsten, M.; von Feilitzen, K.; Forsberg, M.; Persson, L.; Johansson, F.; Zwahlen, M.; von Heijne, G.; Nielsen, J.; Ponten, F. *Science* **2015**, *347*, 1260419.
13. Lenfant, N.; Hotelier, T.; Velluet, E.; Bourne, Y.; Marchot, P.; Chatonnet, A. *Nucleic Acids Res.* **2013**, *41*, D423.
14. Edgar, R. C. *Nucleic Acids Res.* **2004**, *32*, 1792.
15. Lenfant, N.; Bourne, Y.; Marchot, P.; Chatonnet, A. *Chem. Biol. Interact.* **2016**.
16. Baggelaar, M. P.; Chameau, P. J.; Kantae, V.; Hummel, J.; Hsu, K. L.; Janssen, F.; van der Wel, T.; Soethoudt, M.; Deng, H.; den Dulk, H.; Allara, M.; Florea, B. I.; Di Marzo, V.; Wadman, W. J.; Kruse, C. G.; Overkleeft, H. S.; Hankemeier, T.;

- Werkman, T. R.; Cravatt, B. F.; van der Stelt, M. *J. Am. Chem. Soc.* **2015**, *137*, 8851.
17. Ogasawara, D.; Deng, H.; Viader, A.; Baggelaar, M. P.; Breman, A.; den Dulk, H.; van den Nieuwendijk, A. M.; Soethoudt, M.; van der Wel, T.; Zhou, J.; Overkleeft, H. S.; Sanchez-Alavez, M.; Mori, S.; Nguyen, W.; Conti, B.; Liu, X.; Chen, Y.; Liu, Q. S.; Cravatt, B. F.; van der Stelt, M. *Proc. Natl. Acad. Sci. U. S. A.* **2016**, *113*, 26.
18. Hsu, K. L.; Tsuboi, K.; Adibekian, A.; Pugh, H.; Masuda, K.; Cravatt, B. F. *Nat. Chem. Biol.* **2012**, *8*, 999.
19. Long, J. Z.; Cisar, J. S.; Milliken, D.; Niessen, S.; Wang, C.; Trauger, S. A.; Siuzdak, G.; Cravatt, B. F. *Nat. Chem. Biol.* **2011**, *7*, 763.
20. Chen, R.; Yang, L.; McIntyre, T. M. *J. Biol. Chem.* **2007**, *282*, 24842.
21. Navab, M.; Ananthramaiah, G. M.; Reddy, S. T.; Van Lenten, B. J.; Ansell, B. J.; Fonarow, G. C.; Vahabzadeh, K.; Hama, S.; Hough, G.; Kamranpour, N.; Berliner, J. A.; Lusic, A. J.; Fogelman, A. M. *J. Lipid Res.* **2004**, *45*, 993.
22. Yea, K.; Kim, J.; Yoon, J. H.; Kwon, T.; Kim, J. H.; Lee, B. D.; Lee, H. J.; Lee, S. J.; Kim, J. I.; Lee, T. G.; Baek, M. C.; Park, H. S.; Park, K. S.; Ohba, M.; Suh, P. G.; Ryu, S. H. *J. Biol. Chem.* **2009**, *284*, 33833.
23. Murakami, N.; Yokomizo, T.; Okuno, T.; Shimizu, T. *J. Biol. Chem.* **2004**, *279*, 42484.
24. Miyata, K.; Oike, Y.; Hoshii, T.; Maekawa, H.; Ogawa, H.; Suda, T.; Araki, K.; Yamamura, K. *Biochem. Biophys. Res. Commun.* **2005**, *329*, 296.
25. Miyata, K.; Nakayama, M.; Mizuta, S.; Hokimoto, S.; Sugamura, K.; Oshima, S.; Oike, Y.; Sugiyama, S.; Ogawa, H.; Yamamura, K. *Biochem. Biophys. Res. Commun.* **2008**, *365*, 207.
26. Jin, S.; Zhao, G.; Li, Z.; Nishimoto, Y.; Isohama, Y.; Shen, J.; Ito, T.; Takeya, M.; Araki, K.; He, P.; Yamamura, K. *Biochem. Biophys. Res. Commun.* **2009**, *380*, 419.

